P116 from Mycoplasma is a self-sufficient lipid uptake and delivery machinery

Sina Manger[1,5], Serena M. Arghittu[2,5], Lasse Sprankel[1], Jakob Meier-Credo[3], Konstantin Wieland[1], Martin P. Schwalm[4], Daniela Bublak[1], Stefan Knapp[4], Julian Langer[3], Roberto Covino[2*], Achilleas S. Frangakis[1*]

[1]Buchmann Institute for Molecular Life Sciences and Institute for Biophysics, Goethe University, Frankfurt am Main, Germany

[2]Frankfurt Institute for Advanced Studies, IMPRS on Cellular Biophysics, Frankfurt am Main, Germany

[3]Max Planck Institute of Biophysics, Frankfurt, Germany

[4]Buchmann Institute for Molecular Life Sciences, Structural Genomics Consortium and Institute for Pharmaceutical Chemistry, Goethe University, Frankfurt am Main, Germany

[5]These authors contributed equally: Sina Manger, Serena M. Arghittu

*Correspondence: A.S.F. (achilleas.frangakis@biophysik.org) and R.C. (covino@fias.uni-frankfurt.de).

Abstract

Lipid acquisition and transport are fundamental processes in all organisms, but many of the key players remain unidentified. Here, we elucidate the lipid-cycling mechanism of the *Mycoplasma pneumoniae* membrane protein P116. We show that P116 not only extracts lipids from its environment but also self-sufficiently deposits them into both bacterial and eukaryotic cell membranes as well as liposomes. Our structures and molecular dynamics simulation show that the N-terminal region of P116, which resembles an SMP domain, is responsible for perturbing the membrane, while a hydrophobic pocket exploits the chemical gradient to collect the lipids and the protein's dorsal side acts as a mediator of membrane directionality. Furthermore, ligand binding and growth curve assays suggest the potential for designing small molecule inhibitors targeting this essential and immunodominant protein. We show that P116 is a versatile lipid acquisition and delivery machinery that shortcuts the multi-protein pathways used by more complex organisms. Thus, our work advances the understanding of common lipid transport strategies, which may aid research into the mechanisms of more complex lipid-handling machineries.

Introduction

All organisms use membranes to enclose their cells and to organize subcellular compartmentalization. The lipids that form these membranes must be transported into and between membranes by specialized protein-based machineries. Several such machineries have been characterized in recent years, such as the synaptotagmin-like mitochondrial-lipid-binding protein (SMP) domains of the ERMES complex, which tethers the endoplasmic reticulum to the mitochondrium[1], and the extended synaptotagmins (E-Syt), which tether the endoplasmic reticulum to the plasma membrane[2,3]. Another example is the maintenance of lipid asymmetry (Mla) pathway, in which the soluble periplasmic protein MlaC acts as a lipid shuttle to maintain the asymmetrical Gram-negative outer membrane via retrograde phospholipid transport[4,5]. These machineries share some similarities between the domains responsible for lipid uptake, binding and deposition. However, whereas MlaC receives lipids from another protein complex, SMP domains are capable of self-sufficient lipid extraction from membranes[2].

The immunogenic and essential protein P116 from *Mycoplasma*[6] combines a lipid shuttle domain with a large lipid binding cavity. P116 is a homodimer of two 116 kDa monomers that each comprise one core domain, one dimerization domain and one N-terminal domain connected to a transmembrane helix. The core domain has a unique fold that resembles a half-open left hand, with four pairs of amphipathic α-helices, a long α-helix and a five-strand β-sheet forming a huge hydrophobic cavity. Two channels lead into the cavity: the dorsal core access, from the back of the hand; and the distal core access (DCA), which is formed between amphipathic helices 3 and 4, just beneath the N-terminal domain. P116 has a pronounced specificity for lipids that are growth-limiting for *Mycoplasma pneumoniae*, namely phosphatidylcholine (PC),

sphingomyelin (SM) and sterols. *Mycoplasma* species belong to the class of Mollicutes and are characterized by the lack of a cell wall, a small genome, and a reduced metabolism. *M. pneumoniae* adapts its membrane composition to the lipid composition of the culture medium[7,8], but the underlying mechanisms and proteins involved were unknown. Although a structure has been reported for the Mce1 lipid-import machine of a *Mycobacterium tuberculosis* relative[9], studies on cholesterol uptake by other clinically relevant bacteria, such as *Borrelia burgdorferi* and *Helicobacter pylori*, are largely lacking.

Here, we show that the N-terminal domain of P116 resembles the fold of the SMP domains and is essential for binding to and perturbing membranes. We report experimental evidence that P116 can deliver lipids into phospholipid vesicles and eukaryotic cell membranes independently of other proteins. Assays with lipids and other hydrophobic compounds show that P116 binds a variety of hydrophobic molecules but can deliver only lipids, which points to a potential strategy for inhibiting this essential protein. Molecular dynamics (MD) simulations of P116 isolated or in the presence of a membrane as well as free-floating lipids reveal the mechanism of lipid uptake and delivery. To determine the conformation and range of motion of P116 bound on the mycoplasma membrane, we performed cryo-electron tomography on *M. pneumoniae* cells overexpressing P116. Integration of these different approaches reveals that P116 is a compact versatile machinery for lipid extraction and delivery into membranes. Unlike the multi-protein pathways required in more complex organisms, P116 can accomplish these tasks single-handedly.

Results

I. The N-terminal domain is required to extract lipids from membranes.

Purified P116 can self-sufficiently extract lipids from intact membranes

We first set out to demonstrate that the ectodomain of P116 (truncated to amino acids 30–975; this fragment of P116 was used for all single-particle cryo-EM and binding assay experiments unless stated otherwise) is capable of extracting lipids from intact membranes in the absence of other proteins. We incubated empty P116 with dipalmitoylphosphatidylcholine (DPPC) liposomes, removed the liposomes by ultracentrifugation, and confirmed the absence of liposome carryover into the final sample by mass spectrometry. Analysis of the lipid cargo of P116 by mass spectrometry revealed DPPC bound to P116 (Figure 1a). It has previously been shown that P116 can extract lipids from high-density lipoprotein particles and serum in the presence of other lipid-binding proteins and lipoproteins[6]. Here, we show that the soluble ectodomain of P116 alone is capable of perturbing the membrane and extracting lipids, without the involvement of any other proteins.

The N-terminal domain resembles conserved lipid shuttle proteins

Structural comparison with small lipid shuttles suggests that the P116 N-terminal domain may be involved in perturbing membranes, as its fold resembles that of several non-specific lipid transfer proteins. These proteins include sterol carrier protein 2 (SCP2), which appears either isolated or as a part of multidomain proteins in all forms of life[10,11], and the SMP domains, which are part of tether complexes at

membrane contact sites in eukaryotes[1,3] (Extended Data Figure 1). Both SCP2 and SMP domains were recently shown to perturb the membrane and transfer lipids between membranes self-sufficiently[2,11]. Comparison of the amino acid sequences of the P116 N-terminal domain and the E-Syt SMP domain shows poor conservation, with only 14% sequence identity and 25% similarity with 55% gaps (Extended Data Figure 1). However, crucial structural elements of their folds are similar: a large antiparallel β-sheet covers three sides of a hydrophobic channel, while the remaining side is closed by an α-helix (Extended Data Figure 1).

The N-terminal domain is essential for perturbing membranes

To further explore the role of the P116 N-terminal domain in membrane perturbation, we separated it from the rest of the ectodomain. We solved the structure of this truncated P116 construct (246–818) by single-particle cryo-electron microscopy (single-particle cryo-EM) at 4.3 Å (according to the gold-standard criterion of Fourier shell correlation (FSC) = 0.143; EMD-18477; Extended Data Figure 2). The structure resembled the core and dimerization domains of the full-length ectodomain of P116 (30–957; EMD-15274, PDB: 8A9A) (Figure 1b). Using the same lipid extraction experiment carried out on the whole ectodomain, we incubated the emptied construct with DPPC liposomes. After removing the liposomes by ultracentrifugation, we used single-particle cryo-EM to determine the filling state and to verify the structural integrity of the new construct. We obtained the structure of the monomer at 5.43 Å (according to the gold-standard criterion of FSC = 0.143; EMD-18478; Extended Data Figure 2) and determined it to be empty based on the position of the amphipathic helices, which move towards the inside of the cavity when the monomer switches from filled to empty (Figure 1c). Thus, in the absence of the N-terminal domain, extraction of lipids from intact membranes is no longer possible or is much less efficient.

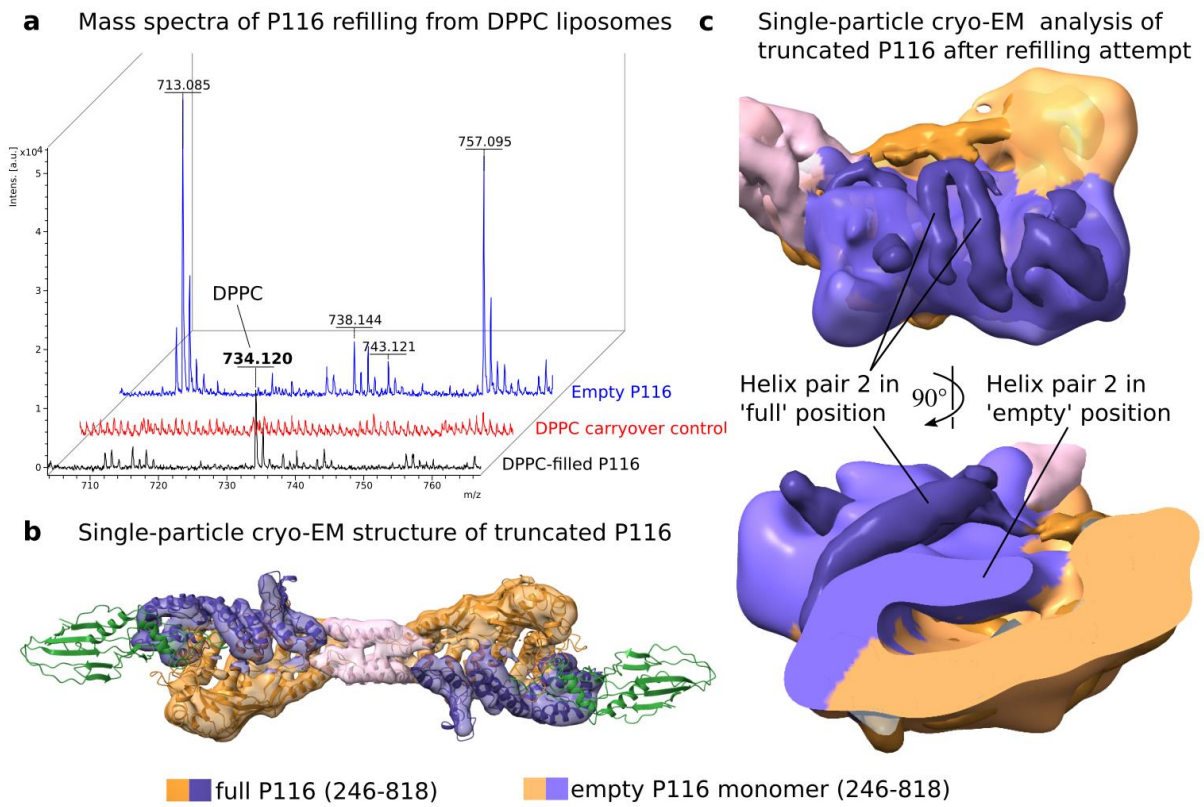

Figure 1: The N-terminal domain of P116 is required to extract lipids from membranes.

a, Mass spectrometry analysis of DPPC extraction from liposomes by P116. Mass spectra of empty P116 (blue; traces of other lipids of mass 713, 738, 743 and 757 Da are visible), DPPC carryover after liposome pelleting (red; no DPPC contamination is visible) and P116 after incubation with and pelleting of DPPC liposomes (black; a clear peak at 734 Da, the mass of DPPC, is visible). The DPPC peak is annotated. Only the final sample of P116 contains DPPC.

b, Single-particle cryo-EM structure of the truncated P116, i.e. without the N-terminal domain, has a similar fold to the full-length protein. The cryo-EM density of P116 without the N-terminal domain (246–818) at 4.16 Å resolution superimposed on the ribbon representation of the filled full-length ectodomain of P116 (60–868) (PDB: 8A9A).

c, The single-particle cryo-EM structure shows that the truncated P116 subjected to the refilling procedure did not take up lipids and stayed in the empty conformation. Superimposition of the P116 (246–818) dimer in the filled state (dark purple, dark orange) with the P116 (246–818) monomer after emptying and refilling (light purple, light orange). Helix pair 2 of the filled conformation is clearly different from the conformation of the truncated P116 monomer density, illustrating that the monomers were not refilled but remained empty.

II. Interaction of P116 with membranes facilitates increased range of motion

Mycoplasma-anchored P116 is highly flexible and mostly not docked to the membrane

Unlike the soluble fragments of P116 that we used for binding assays and MD simulations, native P116 is tethered to the mycoplasma membrane. The N-terminus of each monomer is connected to a single transmembrane helix by a 30 amino-acid linker. The linker is unstructured in the AlphaFold[12] prediction of the protein structure and could not be resolved in our single-particle structure. We hypothesize that the linker would allow for a maximum range of motion between the monomers and the mycoplasma membrane of 10–11 nm. We set out to investigate the conformations of P116 tethered to the mycoplasma membrane by cryo-electron tomography. As each wild-type cell has only ~34 copies of P116[13], we generated an *M. pneumoniae* strain that overexpresses *p116* from its native promoter. The tomograms display cells decorated with P116 particles on their surface (Figure 2a).

Most of the P116 particles seem to adopt a similar conformation, which also emerges in the sub-tomogram average of 700 particles at 30 Å (EMD-18629), in which at least one monomer is positioned at the maximal distance from the membrane that is permitted by the linker (Figure 2b). The sub-tomogram average indicates a pronounced wringing motion between the P116 monomers, as well as a steep incline angle between the core and N-terminal domains on the mycoplasma membrane; an adequate fit of P116 into the average was dependent on both these conformational traits.

Thereby, both the distal and dorsal core access routes as well as the central cleft are at a considerable distance from the membrane and would not allow for either lipid uptake or delivery. Although we could not classify clear conformations due to low particle numbers and the seemingly indiscrete conformations of P116, our manual inspection of the sub-tomograms revealed a noteworthy number of particles in close proximity to or tilted towards the membrane, many of which were interacting with an area of the N-terminal domain larger than just the tip (~ 100 particles, 10% of all selected particles; Extended Data Figure 3). Of particular interest are particles between two adjacent mycoplasma cells that seemingly interact with both membranes (Extended Data Figure 3). Notably, we could identify only a handful of particles (<10) that appeared to interact with the membrane using their dorsal side. However, these particles were too few to allow for a well-resolved sub-tomogram average. In conclusion, tomography of P116 in its native environment on the mycoplasma membrane reveals that P116 is much more conformationally flexible than expected from our single-particle structures.

The preparation method requires that cells are kept in a lipid-free environment for 30 minutes, which was sufficient for lipid delivery by P116 in previous *in vitro* experiments. On this basis, provided that the systems had time to relax to equilibrium, we can conclude that the lipid-starved, membrane-tethered P116 was in a semi-empty state, which hints at a distinct directionality mechanism that prevents lipid extraction from the mycoplasma membrane.

Simulated P116 exhibits larger flexibility when placed close to a membrane

To understand the flexibility of P116 in the vicinity of a membrane and explore the modes of its membrane interaction, we performed coarse-grained MD simulations of the P116 ectodomain (60–868; PDB: 8A9B; this fragment of P116 was used for all

MD simulations). The MD simulations show a broad range of motion, confirming the tomography results (Figure 2c). The motion involves changes to the arc diameter (angle between the monomers), the wringing (rotation of the monomers with respect to each other), and the angle between the N-terminal domain and the core domain. The angle between monomers ranged from an arc diameter of ~12.5 nm in filled P116 to ~11.5 nm in empty P116 in the single-particle structures, while simulated empty P116 reached an arc diameter of up to ~6 nm when placed beside a membrane (Figure 2c, top right). In the single-particle structures of the refilled P116 (EMD-15276), the wringing between monomers was highest at ~45°, while simulated empty P116 displayed a wringing of up to ~125°, which enabled the monomers to face almost opposite directions (Figure 2c, top left). The angle between the N-terminal domain and the core domain was fixed at ~120°–135° in single-particle structures, while it ranged between ~0° and ~125° in simulated empty P116 in the vicinity of a membrane (Figure 2c, bottom). Although the simulations involved the ectodomain of P116 only, the protein continuously interacted with the membrane in multiple different conformations.

MD simulations reveal two distinct modes for membrane docking of P116

Of the range of conformational dynamics performed by P116 (60–868) on the membrane, two main conformations reoccurred over the course of our simulations (Figure 2d):

(i) P116 inserted amino acids F860 and F856 into the membrane, then stabilized the docking through the insertion of F214 and F227. The membrane insertion was maintained for up to 20 μs and placed the DCA right next to the membrane. We refer to this conformation as 'N-docking' (Figure 2d, Extended Data Video 1). F214 and F227 are part of the N-terminal domain β-sheet. In all *Mycoplasma* species, residue 214 is a hydrophobic amino acid, while F227 is conserved. This explains why P116 with a

truncated N-terminal domain (246–818), which is missing all four membrane-anchoring phenylalanines, could no longer extract lipids from membranes. F856 and F860 are situated on the terminal phenylalanine-rich loop (854–860: FAFVDGF) of the core domain, in close proximity to the N-terminal domain. This loop is directly adjacent to the C-terminus in P116 (60–868), the fragment used for all simulations, while P116 (30–957), which we used in all experiments, has ~100 more amino acids at the C-terminus. Therefore, the role of F856, F860, and the rest of the C-terminal fragment requires further investigation.

(ii) P116 interacts with the membrane using its dorsal side, which contains negative charges that attract lipid head groups (Extended Data Figure 4. As the dorsal core access is constantly solvated, it could allow head groups to partially enter the dorsal channel. During the simulations, the membrane curvature is modified as a result of P116 docking with its dorsal core access positioned flat against the membrane. We refer to this conformation as ‘D-docking’ (Figure 2d, Figure 4a, Extended Data Video 1). Notably, in the simulation N-docking of one monomer was preceded by and then coincided with D-docking of the other monomer, indicating a role for D-docking in either initiation of membrane association or differentiation between membranes.

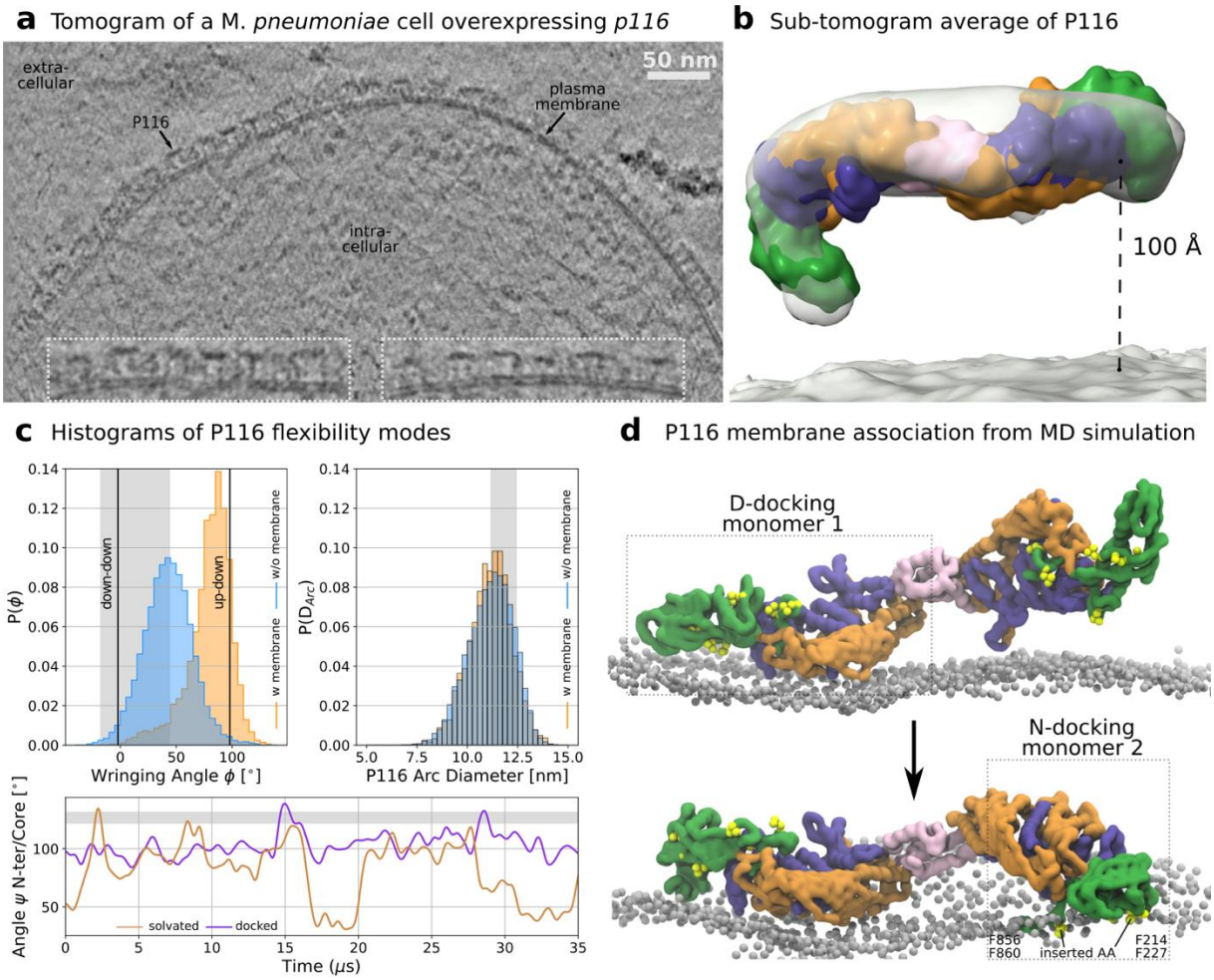

Figure 2: Interaction of P116 with membranes facilitates increased range of motion shown by cryo-ET and MD simulation.

a, Tomographic slice (0.837 Å/pix) of *M. pneumoniae* cells overexpressing *p116* from its native promoter.

b, 30 Å average of 700 particles (grey surface, EMD-18629), overlayed with P116 in a conformation obtained from MD simulations. The distance between the N-terminus and the membrane is 100 Å.

c, Flexibility of P116 (60–868) simulated close to a membrane. The histograms of range of motion from MD simulations show an even larger flexibility than the range of motion observed in single-particle structures of solvated P116 (indicated by grey bars). Three parameters are displayed: The wringing angle (between monomers), the arc diameter (angle between the monomers) and the angle of the N-terminal to the core domain. The wringing between monomers was dramatically increased in the vicinity of a membrane, allowing the monomers to face almost opposite directions. Down-down and up-down refer to the directions the central clefts of each monomer are facing. The angle between the N-terminal domain and the core domain was fixed at ~120°–135° (grey bars) in single-particle structures, while it ranged between 0° and 125° in simulated empty P116 in the vicinity of a membrane. Stable membrane docking restricted the flexibility range of the docked monomer.

d, Renders from MD simulation of P116 (60–868). The attachment of P116 to a membrane involves phenylalanine residues (yellow beads) in the N-terminal domain.

D-docking of monomer 1 precedes N-docking through insertion of F227 and F214 (shown in yellow) of monomer 2. The protein is represented as a filled volume colored by domain. The membrane (DOPG:DOPE:DOPC, 40:30:30) is represented by the phosphate moieties of the lipids, shown as silver beads. Water, ions, and lipid tails are not shown for clarity.

III. P116 self-sufficiently delivers lipids

The P116 ectodomain delivers fluorescent lipids into liposomes *in vitro*

Next, we probed whether P116 can deposit lipids into membranes. We established a fluorescence-based assay using liposomes (Figure 3a), whereby empty P116 was incubated with small (200 nm) fluorescent donor liposomes. The liposomes comprised 30% DOPE labelled with a Dansyl-fluorophore at the head group, 30% DOPC labelled with an NBD fluorophore in one acyl chain, and 40% DOPG (Figure 3c). The donor liposomes were then removed by ultracentrifugation. The absence of relevant carryover was confirmed by mass spectrometry. The P116 loaded with fluorescent lipids was subsequently incubated with large DPPC acceptor liposomes (> 1 μm) overnight at ambient conditions. In the final step, P116 was removed by ultrafiltration, and its absence was confirmed with a dot blot. The remaining DPPC liposomes were imaged by fluorescence microscopy. The auto-fluorescence of the acceptor liposome was measured along with the fluorescence signal of a control to account for spontaneous transfer of lipids or fusion of liposomes as a result of potential carryover of fluorescent donor liposomes (Figure 3b-d, Extended Data Figure 5).

The DPPC acceptor liposomes displayed an intense fluorescence signa (Figure 3b 1). The signal in both controls was statistically significantly less (Extended Data Table 1): in the NBD channel, no signal was detected in either control; and in the Dansyl channel, both controls displayed some (auto) fluorescence signal. Thus, NBD-DOPC and Dansyl-DOPE were both delivered into the DPPC acceptor liposomes

independently of whether the fluorophore was placed in the head or the tail group. Liposome carryover below the sensitivity range of the mass spectrometry control may be present, and spontaneous transfer was not detected for NBD-DOPC but was found to some extent for Dansyl-DOPE. The latter can be explained by the position of the Dansyl fluorophore on the PC head group, which changes the head group from hydrophilic to amphiphilic. The absence of an NBD-DOPC signal in the control confirms that fusion of carryover fluorescent donor liposomes and DPPC acceptor liposomes did not occur. The carryover fluorescent donor liposomes could not have been mistaken for acceptor liposomes, because they are at least five-fold smaller, which is below the resolution limit of the light microscope. The experiment was carried out in triplicate, and all results could be replicated. Analysis of the DPPC liposomes with mass spectrometry instead of fluorescence microscopy yielded the same result. Hence, the ectodomain of P116 can deposit its lipid cargo into a phospholipid membrane without being tethered to the mycoplasma membrane and without requiring other proteins.

To explore whether P116 can also deliver its cargo in living cells, we incubated P116 filled with fluorescent lipids together with adherent HaCaT cells in serum-free DMEM medium overnight, for 2 h or for 30 minutes at 37°C, before removing the P116 by washing. While prolonged treatment with P116 caused the cells to disintegrate, comparable to harsh detergent treatment, cells treated for 30 minutes displayed intense fluorescence (Figure 3b 2). This finding indicates that P116 extracted lipids from the eukaryotic cells after delivering its fluorescent cargo.

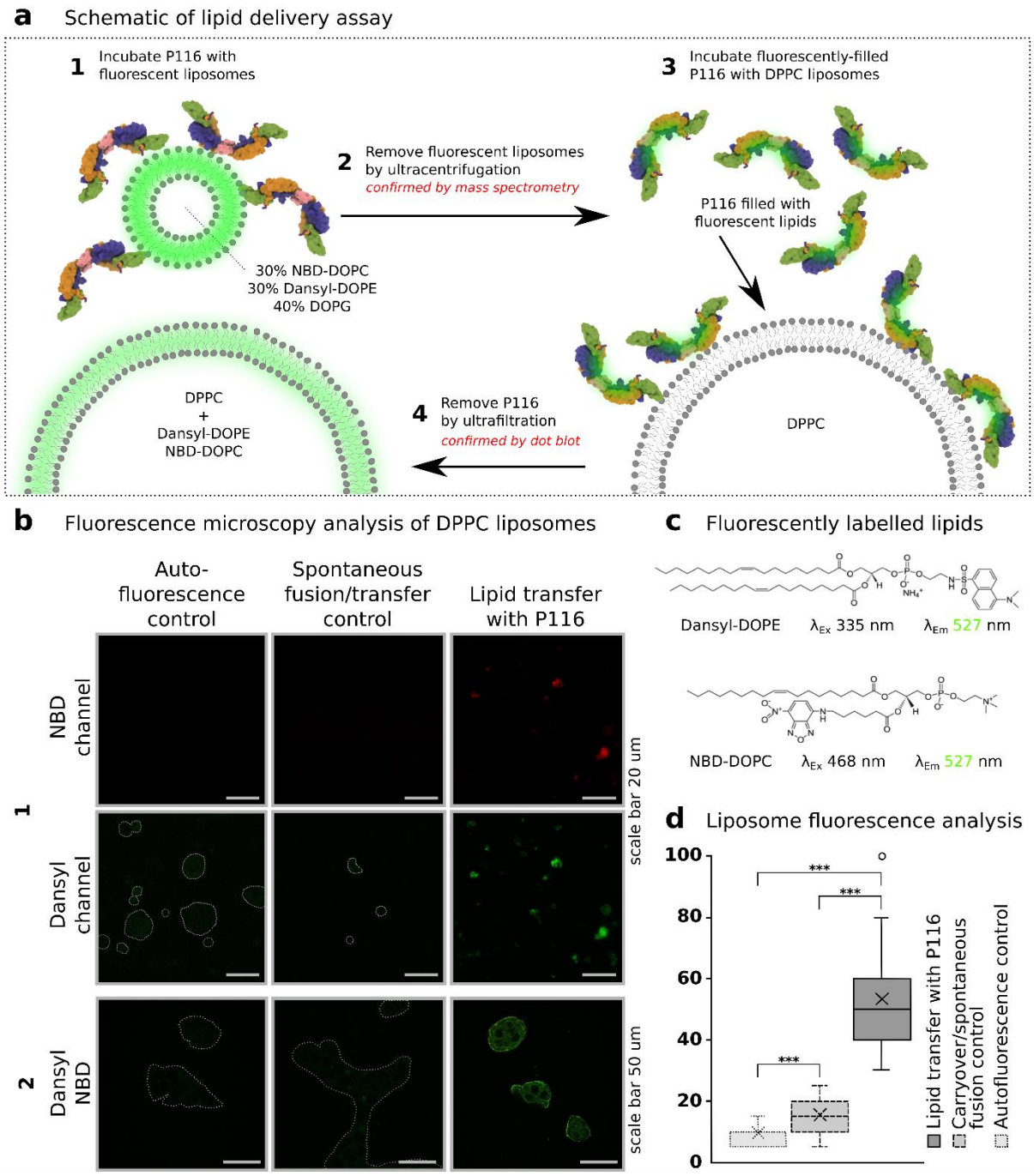

Figure 3: P116 self-sufficiently and single-handedly delivers lipids.
a, Schematic of lipid delivery assay. 1) Incubation of empty P116 with fluorescent donor liposomes. 2) Removal of donor liposomes by ultracentrifugation and verification of removal by mass spectrometry. 3) Incubation of now fluorescently filled P116 with non-fluorescent DPPC acceptor liposomes. 4) Removal of P116 by ultrafiltration and verification of removal by dot blot, followed by analysis of fluorescent traits of acceptor liposomes by laser-scanning microscopy.
b, Representative confocal light microscopy images. 1) Delivery into DPPC liposomes. 2) Delivery into HaCaT cells. (Left) Liposomes/cells (auto-fluorescence control), (middle) sample from the same workflow without P116 (spontaneous fusion/transfer control), and (right) sample with P116, according to the workflow detailed in **a** (lipid transfer with P116). The Dansyl and NBD channels are shown separately because of

the large difference in excitation maxima and resulting use of separate laser lines. Both fluorophores emit in the green spectrum (at 527 nm). The NBD fluorescence signal is shown in red to facilitate interpretation of the merged image.
c, Fluorescent lipids used in donor liposomes with their excitation and emission maxima.
d, Statistical analysis of fluorescence differences between the sample in the presence of P116 and the controls. All differences are statistically significant. The experiment was carried out in triplicate, and all results could be replicated. The 25–75% data range is contained in the box, the horizontal line represents the median, the vertical line represents range within 1.5 interquartile range, the X represents the mean, and the circle represents outlier. Data can be found in Extended Data Table 1.

IV. The mechanism of lipid uptake and delivery

The DCA and the membrane are perturbed in N-docking but not in D-docking

Both N-docking and D-docking place the DCA near the membrane (Figure 4a & b). During N-docking, the part of the DCA that can open and close (hereafter referred to as the gate) faces the membrane, and an opening of the gate was repeatedly observed (Figure 4b & c). By contrast, during D-docking, the DCA is placed on the membrane with the tip facing down, and no opening was observed. In addition, the membrane below the docked monomer opens widely during N-docking but not D-docking (Figure 4d).

Simulated P116 takes up DOPE lipids via the DCA

To determine the mechanism by which lipids enter P116, we performed an MD simulation of empty P116 with DOPE and DOPG lipids solvated and evenly distributed in the box. This far-from-equilibrium initial condition enabled us to sample the interactions between P116 and the lipids efficiently. The simulation revealed two very fast events: (i) the formation of micelle-like lipid aggregates; and (ii) the uptake of a

lipid through the previously closed DCA of one monomer. The lipid on the outside of the DCA was caged by F860, F856, F854 and F87 (Figure 4e 1, right). Notably, F860 and F856 were inserted into the membrane in the previous simulation. Lipid uptake was initiated by the flipping of one hydrophobic tail into the DCA followed by the other. The hydrophilic head group remained on the outside of the cavity until the lipid fully entered the channel, making room for more lipids at the DCA (Figure 4e 2, right, Extended Data Video 2). Once the lipid entered the main cavity, it positioned its head group towards the central cleft and the dorsal core access. When we placed a lipid in the observed split position in the gap between the membrane and the DCA of an N-docked P116, instead of falling back into the membrane, it was taken up by P116 (Figure 4e 2). This suggests that lipid uptake as described above could also occur directly from a membrane.

Both lipid caging and membrane insertion required a high flexibility of the N-terminal domain, as shown in Figure 2. When the flexibility was restricted to the range seen in single-particle cryo-EM structures, neither N-docking nor placement of lipids at the DCA occurred.

In addition to entering through the DCA into the central cavity, a DOPE molecule also entered the hydrophobic channel of the N-terminal domain, and lipid micelles attached to different parts of the N-terminal domain, which thus proved to be attractive to micelles and lipids (Extended Data Video 2). The phenylalanine residues that were inserted during N-docking (F227 and F214) were involved in binding the lipid within the N-terminal domain.

Simulation of P116 with cholesterol cargo shows positioning of cholesterol at the DCA

To further study what happens with cargo inside the hydrophobic cavity of P116, we performed an atomistic MD simulation of P116 filled with 12 cholesterols per monomer. First, the amphipathic helices squeezes the cargo into the cavity towards the dimerization domain. This is expected, as the cavity must always be as closed as possible in the filled state to avoid exposing hydrophobic residues to the solvent. Next, one cholesterol molecule inserts in the DCA, with the hydroxyl group positioned towards the solvent. Over the course of the simulation, the cholesterol molecule falls back into the cavity, while being replaced by another cholesterol molecule (Figure 4f).

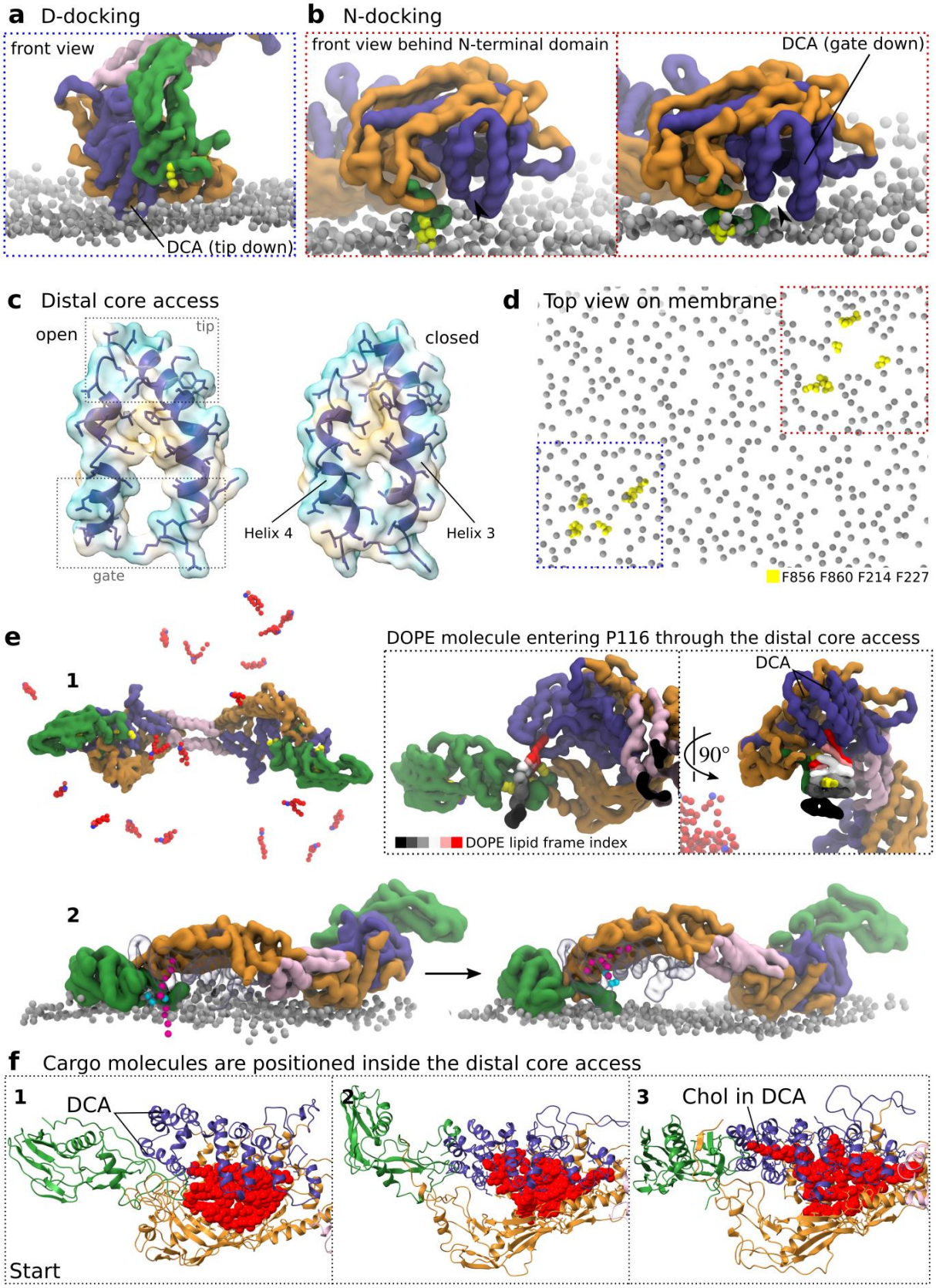

Figure 4: MD simulation reveals mechanism of lipid uptake and delivery by P116. In all simulation renders, P116 is represented by a filled volume or cartoon representation colored by domain. When present, the membrane is indicated by the phosphate moiety (represented by silver beads) and solvated lipids are represented

by phosphate moieties (blue beads) and tails (red beads). Water and ions are not shown for clarity.
a, D-docking places the tip of the DCA near the membrane.
b, N-docking places the gate of the DCA near the membrane when closed (left) and opened (right). Residues F860, F856, F227 and F214, which insert into the membrane, are shown as yellow beads.
c, Details of DCA architecture show opening at the gate side only. Comparison of the DCA conformation between the filled and empty single-particle cryo-EM structures (PDB: 8A9A and 8A9B, respectively). The two helices comprising the DCA are shown in blue with the individual amino acid sidechains as stick models. The surface representations are colored by hydrophobicity factor (yellow is hydrophobic and blue is hydrophilic). The DCA opens and closes at the gate side while the tip side remains closed.
d, N-docking promotes opening of the membrane below the DCA. Top view of the membrane during double docking of P116 (P116 not shown for clarity). The D-docking area is labelled with a blue box, the N-docking area with a red box. Residues F860, F856, F227 and F214 are shown as yellow beads. The membrane barrier is perturbed only during N-docking, which promotes opening of the membrane below the DCA.
e, Lipids enter the DCA in a split position. **e_1** Coarse-grained MD simulation of P116 with free-floating DOPE, DOPC and DOPG lipids. F860, F856, F227 and F214 are shown as yellow beads. (Left) Start of simulation with evenly distributed lipids. (Right) DOPE lipid entering the cavity through the DCA. The lipid is shown as a filled volume colored according to the trajectory frame. **e_2** (Left) N-docked P116 with DOPE lipid in split position placed below the DCA. (Right) DOPE lipid entering the cavity through the DCA. The taken-up lipid is represented by beads, head group in cyan and tail in magenta for contrast. The DCA and finger helices of the monomer involved in N-docking and uptake are rendered as transparent shapes for clarity.
f, Cargo inside the cavity is positioned inside the DCA. Atomistic MD simulation of 12 cholesterol molecules (shown as red spheres) in the cavity of P116. **f_1** Start of simulation with cholesterol molecules evenly distributed inside the cavity. **f_2** Cholesterol molecules rearrange and are squeezed into the cavity towards the dimerization domain. **f_3** An individual cholesterol molecule inserts in the hydrophobic channel formed by the DCA.

V. P116 gets clogged by large compounds

P116 binds hydrophobic compounds inside its cavity but does not deliver them

Based on the observation that the architecture of the DCA is not particularly selective, we next investigated the capabilities of P116 to take up and delivery non-

lipid hydrophobic compounds, potentially acting as a drug delivery system. In addition to a peptide, we chose a number of hydrophobic bifunctional small molecules that can be used as PROTACs (proteolysis targeting chimeras) to selectively degrade proteins of interest in cellular environments and *in vivo*. Due to their large size, PROTACs have been associated with less favorable pharmacological properties due to unfavorable solubility and cell penetration[14,15]. We incubated empty P116 with six compounds ranging in size from 1.0 to 2.4 kDa (1.0, 1.1, 1.2, 1.3, 1.7 and 2.4 kDa) (Figure 5a' & b', Extended Data Figure 6 a'-f'). Unbound compound was removed by ultrafiltration, and P116 was analyzed by mass spectrometry (Figure 5a & b, Extended Data Figure 5a-f). All compounds were bound to P116, but the largest compound had a much lower binding affinity than did the smaller compounds. This supports the finding from MD simulations that the DCA is the single entry and exit point of P116, as the 2.4 kDa compound would just barely be able to squeeze through the channel when it is fully opened.

To confirm that the compounds were bound inside the hydrophobic cavity of P116, we determined the structure of P116 with the 1.7 kDa compound (Figure 5b') by single-particle cryo-EM at 3.3 Å (according to the gold-standard criterion of FSCS = 0.143; EMD-18476; Extended Data Figure 2). The compound, a peptide, was clearly located within the cavity, while the conformation of P116 was similar to that of the lipid-filled protein (EMD-15274; Figure 5d). The result of this assay demonstrates that P116 can bind ligands with a broad range of sizes, overall shapes, and distributions of hydrophilic and hydrophobic parts.

We then performed the lipid delivery assay with P116 filled with the same six compounds, however, none of the compounds were delivered into the membranes. Aside from their size and shape, the compounds differ from lipids by the distribution of

hydrophilic and hydrophobic parts, which is likely the cause of their incompatibility with the lipid delivery machinery.

Next, we tested whether these six compounds can in fact inhibit the growth of cultured mycoplasma cells. When each compound was added directly to the cell culture, no effect was visible, indicating that non-lipid compounds are not taken up by P116 when in direct competition with an excess of lipids in the growth medium. When the cells were washed and kept in PBS for 30 minutes, then incubated with compound a or b (Figure 5a' & b'; the control was treated with DMSO) in PBS for another 30 minutes, a growth delay was observed (Figure 5c). This suggests that the compounds, once bound to P116, could not be replaced by the lipids in the medium. It also indicates that P116 did not efficiently extract lipids from the mycoplasma membrane after delivering its cargo, but instead remained in a semi-empty state, ready to extract cargo from the environment.

Interestingly, the cell growth resumed after one cell division cycle when the cells were placed back into the normal growth medium. This observation can be explained by the replacement of inactive P116 on the plasma membrane[16,17]. These data suggest that hydrophobic peptides may act as growth inhibitors of *M. pneumoniae*, even though the development of higher-affinity compounds that can compete with lipids would be needed for effective *in vivo* use.

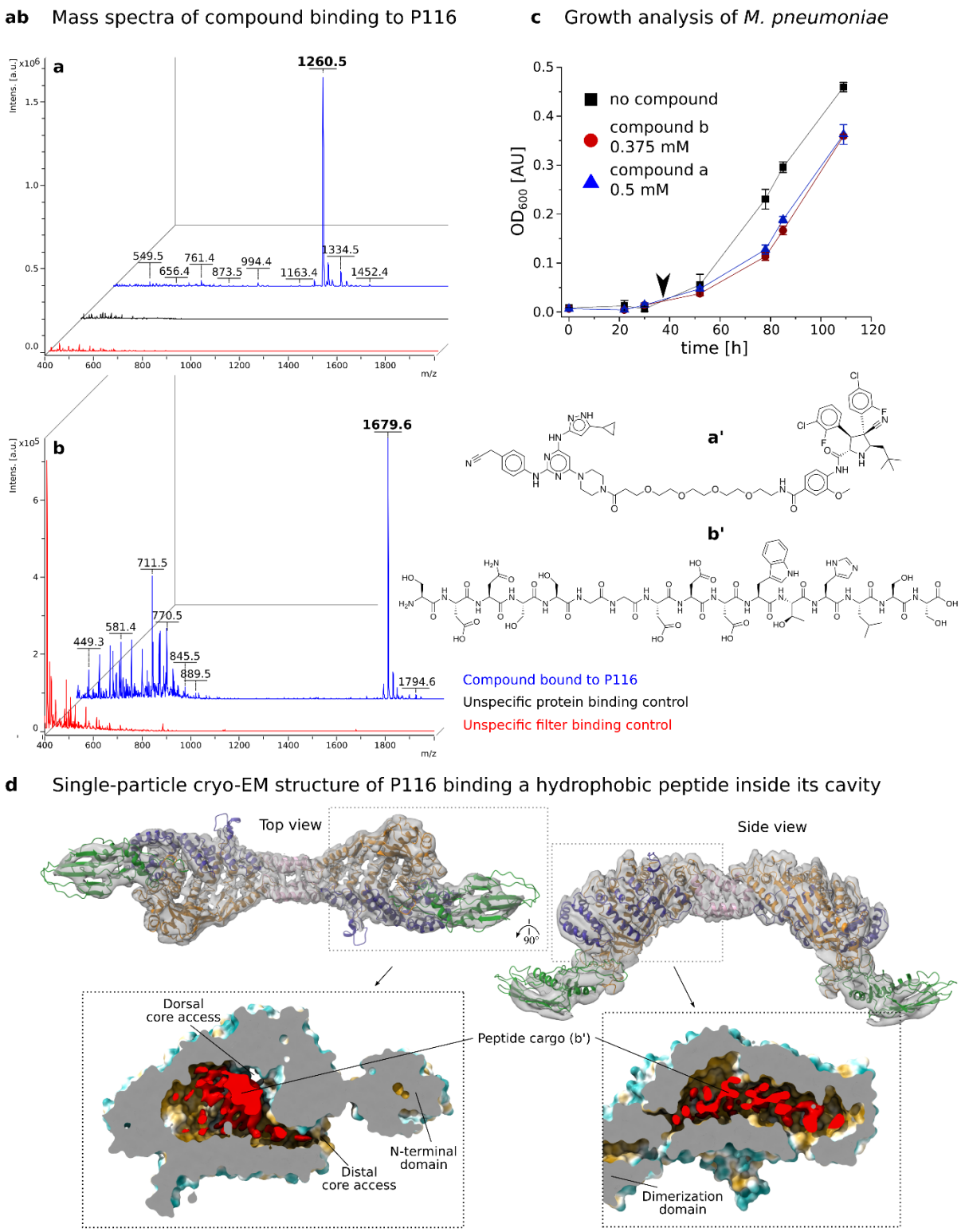

Figure 5: Analysis of PROTACs and hydrophobic peptide binding by P116.
ab, Mass spectra show that compounds are specifically bound by P116. Compounds bound to P116 (blue), to P110 or P140 (other mycoplasma membrane proteins, black) or to the filter (red).
a'b', Structures of (a) a PROTAC and (b) a hydrophobic peptide that were used to load P116. Peaks corresponding to each compound are annotated in bold in the respective spectrum.

c, The growth of cultured mycoplasma cells is inhibited by the tested compounds. Growth curves of *M. pneumoniae* treated with compound b' (red), compound a' (blue) and DMSO (black) in PBS at 35 h growth for 30 min before re-culturing in medium. The time of compound treatment is indicated with a black arrow. The experiment was carried out in triplicate, and all results could be replicated. Error bars represent standard deviation.
d, Single-particle cryo-EM structure of P116 filled with hydrophobic peptide b'. The grey surface shows the density of peptide-filled P116 at 3.3 Å. It was fitted with the structure of P116 in the filled state (colored ribbon model, PDB: 8A9A). The surface representation in the lower panels is colored by hydrophobicity factor (yellow is hydrophobic and blue is hydrophilic) with the sectioning surface in grey. The peptide inside the hydrophobic cavity of P116 is colored red.

Discussion

Mycoplasmas have evolved a minimal lipid transport system composed of a single protein that can self-sufficiently acquire and deliver lipids. Importantly, as ATP is not involved in the lipid transport (all experiments were performed in the absence of ATP), uptake and delivery must be driven by a lipid concentration gradient. Our structural and simulation data show that the SMP-like N-terminal domain of P116 perturbs the membrane by stably inserting two phenylalanine residues (Figure 2d, Extended Data Figure 1), while the core domain, consisting of a huge hydrophobic pocket, creates a steep energetic slide for collecting lipids. Delivery is facilitated by the difference in lipid composition between the target membrane and the lipid cargo inside the hydrophobic pocket. The lipids will slide towards the hydrophobic core, which exerts the largest force: towards the cavity when the pocket is empty to equilibrate the lipid concentration, and towards the membrane when the pocket is filled.

Our simulations reveal that N-docking facilitates membrane association, while D-docking appears to be necessary for the directionality of lipid transport (Figure 6). The membranes of mycoplasmas and eukaryotic cells differ by their lipid composition

and surface charge. Mycoplasma membranes comprise approximately 30% anionic lipids, whereas the outer leaflet of eukaryotic cells is neutral and contains mostly cholesterol, PC and SM[18,19]. As a result, the predominantly negatively charged dorsal side of P116 preferably attaches to the host cell membrane (Extended Data Figure 5d). This is supported by the finding that P116 faces high-density lipoprotein particles with its dorsal side[6]. Thus, we conclude that lipid uptake from the host by empty P116 via simultaneous D- and N-docking of both monomers is more efficient compared to lipid uptake from its own mycoplasma membrane. In the filled state, when P116 is more rigid, the two docking modes cannot coincide on the same membrane; simultaneous D- and N-docking mandates a wringing angle of ~100°, but the maximum wringing angle observed in single-particle structures of filled P116 was ~45°. Thereby, the probability of delivery into the host membrane is reduced (Figure 6). Unlike in SMP domains[2], the membrane-sensitive residues of P116 (D-docking) are not adjacent to the binding interface (N-docking). Whether both monomers can face the membrane simultaneously depends on the filling state of the protein, which effectively enables the interdependency of membrane directionality. After uptake from the host, delivery into the mycoplasma membrane is incentivized by the lipid composition gradient between the cargo inside P116 and the mycoplasma membrane. Considering the presence of the membrane linker, which stochastically increases the opportunity for membrane association, delivery into the mycoplasma membrane seems more likely.

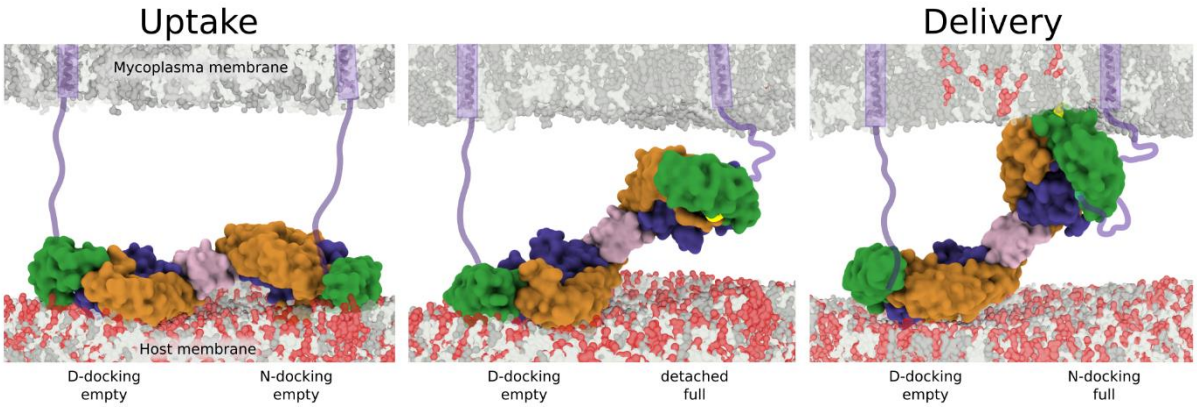

Figure 6: Cartoon of uptake and delivery mechanism in P116.
When empty, P116 is flexible enough to dorsally dock one monomer while distally docking the second monomer. The dorsal docking happens first, as it is based on long-range electrostatic interactions, which brings the second monomer close enough to the membrane to insert several phenylalanine residues (shown in yellow). Lipids enter P116 through the DCA **(left)**. Lipids inside the cavity are not shown. After the second monomer is filled, lipid head groups bind to residues in the dimerization domain, reducing the overall flexibility and possibly causing the monomer to detach **(middle)**. We propose that the filled monomer can now dock with the mycoplasma membrane and deliver its lipids through the DCA, following the concentration gradient **(right)**.

Our insights into the lipid acquisition mechanism in *M. pneumoniae* may contribute to advancing the understanding of more complex lipid transport pathways in other bacteria and eukaryotes. These findings may also facilitate the development of a small molecule inhibitor as a growth-inhibiting agent both in eukaryotic cell culture and to combat mycoplasma infections in a clinical setting.

Data Availability

The single-particle cryo-EM structures solved in this study are available at http://www.emdataresource.org/ under EMD-18476, EMD-18477, EMD-18478 and EMD-18629 (Extended Data Table 2).

The MD data that support the findings of this study, including Extended Data Videos 1 & 2, are available in MD_P116 at http://doi.org/10.5281/zenodo.8389183.

Acknowledgements and Funding

We thank the Frankfurt Center for Electron Microscopy and the Frankfurt Center for Advanced Light Microscopy for measurement time. We thank the Central Electron Microscopy Facility at the MPI of Biophysics in Frankfurt, which enabled us to collect the tomography dataset as well as the single-particle dataset of empty P116 monomers, particularly S. Welsch and S. Prinz who assisted during the data collection. We thank N. Morgner and J. Schulte for their support during LILBID mass spectroscopy measurements, C. Glaubitz and I. Weber for assistance with liposome preparation, I. Fita, D. Vizarraga and J. Martín for the kind provision of purified P116 (246–818), M. Kunz for support with tomogram reconstruction, and A. N. Birtasu and U. H. Ermel for assistance with sub-tomogram averaging. We thank Jörg Stülke *for providing the M. pneumoniae* replicating plasmid pGP2756[20]. We thank Ignacio Fita/Jesús Martín for gifting us vector pOPINE_P116 . We thank M. R. Vabulas for valuable discussions and comments. S.M. A. and R.C. acknowledge the support of the Frankfurt Institute of Advanced Studies, the LOEWE Center for Multiscale Modelling in Life Sciences of the state of Hesse, the CRC 1507: Membrane-associated Protein Assemblies, Machineries, and Supercomplexes (P09), and the International Max Planck Research School on Cellular Biophysics, as well as computational resources and support from the Center for Scientific Computing of the Goethe University and the Jülich

Supercomputing Centre. A. S. F. acknowledges support from the Deutsche Forschungsgemeinschaft (FR 1653/6-3 for L.S., SFB 902 for K.W. and D.B.) and the Research Training Group iMOL (GRK 2566/1 for S.M).

Author contributions

S.M.: Expressed and purified P116 (30–957), optimized and carried out emptying protocol, established and carried out cargo binding and delivery assays, prepared samples for single-particle analysis, established and cultured P116 overexpression strain of *M. pneumoniae*, prepared samples for tomography, carried out growth curve analyses of *M. pneumoniae* with hydrophobic compounds, recorded and processed single-particle dataset of empty P116 (246–818) monomers. S.M.A: Planned and carried out all MD simulations and MD data analysis. S.M. and L.S.: Recorded and processed single-particle dataset of filled P116 (246–818), recorded and processed tomography dataset of *M. pneumoniae* P116 overexpression strain. L.S.: Recorded and processed single-particle dataset of peptide-filled P116 (30–957). J.M.-C.: Performed mass spectrometry analyses of all samples from cargo binding and delivery assays. K.W. and S.M.: Carried out laser scanning microscopy on samples from delivery assays. M.P.S.: Performed NanoBRET analyses of hydrophobic compound delivery. D.B.: Assisted with expression and purification of P116 (30–957), emptying and refilling protocols, and cargo binding and delivery assays. S.K.: Provided hydrophobic compounds, supervised research. J.L., R.C. and A.S.F.: Designed and supervised research. S.M. and A. S. F.: Wrote the manuscript, with contributions from all authors.

Competing interests

The authors declare no competing interests.

References

1. AhYoung, A. P. *et al.* Conserved SMP domains of the ERMES complex bind phospholipids and mediate tether assembly. *Proceedings of the National Academy of Sciences of the United States of America* **112,** E3179-88; 10.1073/pnas.1422363112 (2015).
2. Wang, Y. *et al.* Insights into membrane association of the SMP domain of extended synaptotagmin. *Nature Communications* **14**; 10.1038/s41467-023-37202-8 (2023).
3. Schauder, C. M. *et al.* Structure of a lipid-bound extended synaptotagmin indicates a role in lipid transfer. *Nature* **510,** 552–555; 10.1038/nature13269 (2014).
4. Hughes, G. W. *et al.* Evidence for phospholipid export from the bacterial inner membrane by the Mla ABC transport system. *Nature Microbiology* **4,** 1692–1705; 10.1038/s41564-019-0481-y (2019).
5. Ekiert, D. C. *et al.* Architectures of lipid transport systems for the bacterial outer membrane. *Cell* **169,** 273-285.e17; 10.1016/j.cell.2017.03.019 (2017).
6. Sprankel, L. *et al.* Essential protein P116 extracts cholesterol and other indispensable lipids for Mycoplasmas. *Nature Structural & Molecular Biology* **30,** 321–329; 10.1038/s41594-023-00922-y (2023).
7. McElhaney, R. N. & Tourtellotte, M. E. Mycoplasma membrane lipids: variations in fatty acid composition. *Science (New York, N.Y.)* **164,** 433–434; 10.1126/science.164.3878.433 (1969).
8. Archer, D. B. Modification of the membrane composition of Mycoplasma mycoides subsp. capri by the growth medium. *Journal of General Microbiology* **88,** 329–338; 10.1099/00221287-88-2-329 (1975).
9. Chen, J. *et al.* Structure of an endogenous mycobacterial MCE lipid transporter. *Nature*; 10.1038/s41586-023-06366-0 (2023).
10. Gianotti, A. R., Klinke, S. & Ermácora, M. R. The structure of unliganded sterol carrier protein 2 from Yarrowia lipolytica unveils a mechanism for binding site occlusion. *Journal of Structural Biology* **213,** 107675; 10.1016/j.jsb.2020.107675 (2021).
11. Burgardt, N. I., Gianotti, A. R., Ferreyra, R. G. & Ermácora, M. R. A structural appraisal of sterol carrier protein 2. *Biochimica et Biophysica Acta. Proteins and Proteomics* **1865,** 565–577; 10.1016/j.bbapap.2017.03.002 (2017).
12. Jumper, J. *et al.* Highly accurate protein structure prediction with AlphaFold. *Nature* **596,** 583–589; 10.1038/s41586-021-03819-2 (2021).
13. Yus, E. *et al.* Impact of genome reduction on bacterial metabolism and its regulation. *Science (New York, N.Y.)* **326,** 1263–1268; 10.1126/science.1177263 (2009).
14. Schwalm, M. P. *et al.* Tracking the PROTAC degradation pathway in living cells highlights the importance of ternary complex measurement for PROTAC optimization. *Cell Chemical Biology* **30,** 753-765.e8; 10.1016/j.chembiol.2023.06.002 (2023).
15. Dölle, A. *et al.* Design, Synthesis, and Evaluation of WD-Repeat-Containing Protein 5 (WDR5) Degraders. *Journal of Medicinal Chemistry* **64,** 10682–10710; 10.1021/acs.jmedchem.1c00146 (2021).
16. Kahane, I. & Razin, S. Synthesis and turnover of membrane protein and lipid in Mycoplasma laidlawii. *Biochimica et Biophysica Acta* **183,** 79–89; 10.1016/0005-2736(69)90131-X (1969).
17. Maier, T. *et al.* Quantification of mRNA and protein and integration with protein turnover in a bacterium. *Molecular Systems Biology* **7,** 511; 10.1038/msb.2011.38 (2011).

18. Gaspari, E. *et al.* Model-driven design allows growth of Mycoplasma pneumoniae on serum-free media. *NPJ Systems Biology and Applications* **6**; 10.1038/s41540-020-00153-7 (2020).

19. Casares, D., Escribá, P. V. & Rosselló, C. A. Membrane Lipid Composition: Effect on Membrane and Organelle Structure, Function and Compartmentalization and Therapeutic Avenues. *International Journal of Molecular Sciences* **20**; 10.3390/ijms20092167 (2019).

Material & Methods

Overexpression of native P116 in *M. pneumoniae*

The gene *mpn213* (coding for P116) was amplified from isolated genomic DNA of *M. pneumoniae* strain M129 using primers 5' CAGGACTCGAGCCGTTTGTTTAAGGACAA-AAC 3' and 5' GGAGATATCCTAAAAACCAACGAACCAGAAG 3', bearing an EcoRV and a XhoI restriction site, respectively. As little is known about Mycoplasma promoters and enhancers, the position of the forward primer was chosen at the end of *mpn212*, upstream of *mpn213*, to include the native promoter and regulatory elements. The *M. pneumoniae* replicating plasmid pGP2756[20], was linearized by PCR using primers 5' CTGAGATATCTAGTTATTG-CTCAGCGGTGG 3' and 5' CAGGACTCGAGCACTTTTCGGGGAAATGTGC 3', bearing an EcoRV and a XhoI restriction site, respectively. After restriction with the respective enzymes, the linearized backbone and amplified gene were ligated and used to transform DH5α *Escherichia coli* cells. The resulting plasmid is available upon request.

After verification by sequencing, *M. pneumoniae* cells were transformed as previously described[21]: *M. pneumoniae* cultures were grown to late-exponential phase in 75 cm^2 culture flasks. The adherent cell layer was washed three times with chilled electroporation buffer (8.0 mM HEPES, 272 mM sucrose, pH 7.4), scraped off and resuspended in 0.5 mL of the same buffer. The suspension was passed ten times though a 25-gauge syringe needle. Then, 200 µL aliquots were mixed with 1 µg of the plasmid and transferred to 0.2 cm electro cuvettes (BIO-RAD, Hercules, USA), chilled for 15 min on ice, and electroporated in a BIO-RAD MicroPulser Electroporator using the Ec2 preset (2500 V). After pulsing, the cells were chilled on ice for 15 min before 600 µL of prewarmed SP4 medium was added. Cells were allowed to recover at 37°C for 2 h before the transformation volume was inoculated into a 75 cm^2 tissue culture

flask filled with 20 mL medium containing 10 µg/mL tetracycline and further cultured at 37°C.

Growth curve analysis of *M. pneumoniae*

M. pneumoniae cultures were grown for 30 h in culture dishes (TC dish 35 cell+; Sarstedt, Nümbrecht, Germany). The adherent cell layer was washed three times with PBS, left in PBS for 30 min, scraped off and resuspended in 1 mL PBS, pelleted at maximum speed in a tabletop centrifuge for 20 min and resuspended in 200 µL PBS containing: 20 µL DMSO, 500 µM compound d in 20 µL DMSO, or 375 µL compound e in 15 µL DMSO. Each suspension was passed five times though a 25-gauge syringe needle and incubated for 30 min at 37°C. Each suspension was then inoculated in 4 mL medium and, after thorough mixing, divided into four parts and re-cultured at 37°C. Dishes were retrieved at 52, 78, 85 and 109 h, respectively, and cells were scraped off and passed five times though a 25-gauge syringe needle. A 1 mL volume of the suspension was used for OD_{600} measurement. The experiment was performed with three biological replicates for each condition, and the OD_{600} measurement was performed with three technical replicates. All results could be replicated.

Expression and purification of P116

The extracellular domain of P116, C-terminally shortened and HIS-tagged (30–957), was expressed via the vector pOPINE_P116 backbone #26043; Addgene, Watertown, USA). The vector is available upon request. *E. coli* BL21 (DE3) cells harboring the vector were grown at 37°C to an OD_{600} of 0.6, induced with 0.6 mM IPTG and further grown overnight at 20°C with mild shaking. Cells were harvested, lysed by sonication in lysis buffer (50 mM Tris-HCl, pH 7.4, 20 mM imidazole, 1 mM PMSF) and centrifuged at 20,000 x g in a tabletop centrifuge for 45 min at 4°C. The supernatant

was loaded onto a HisTrap 5 mL column (GE Healthcare, Chicago, USA) that was pre-equilibrated in binding buffer (20 mM Tris-HCl, pH 7.4, 20 mM imidazole), thoroughly washed in binding buffer and eluted with elution buffer (20 mM Tris-HCl pH 7.4, 400 mM imidazole, 150 mM NaCl). The eluate was loaded onto a Superose 6 column (GE Healthcare, Chicago, USA) in protein buffer (20 mM TRIS-HCl, pH 7.4, 150 mM NaCl). Fractions containing non-aggregated P116 were pooled and stored at –80 °C.

Emptying of P116

To obtain empty P116, we added 2.6% Triton X-100 to the protein sample and incubated it for either 1.5 h at room temperature (full-length P116) or 3 h at 37°C (construct without the N-terminal domain) with shaking. The Triton X-100 was then removed by either (i) binding to a HisTrap 1 mL column (GE Healthcare, Chicago, USA) or HIS-Select Nickel Affinity Gel in a gravity-flow column (Merck, Darmstadt, Germany), followed by washing with binding buffer with and without 1.3% Triton X-100, before eluting the samples from the column; or (ii) diluting twice to 15 mL and then to 95% concentration in a centrifugal concentrator (Pierce, 50,000 MWCO PES; Thermo Fischer Scientific, Waltham, USA) and subsequently running through a detergent removal spin column (Pierce; Thermo Fischer Scientific, Waltham, USA). P116 was concentrated using Vivaspin 500 centrifugal concentrators (10,000 MWCO PES; Sartorius, Göttingen, Germany) to a final concentration of >0.5 mg/mL.

Preparation of liposomes

Generally, lipids were dissolved in chloroform, then mixed and dried under nitrogen followed by high vacuum overnight. The dried lipid mixtures were then slowly dispersed in liposome buffer (20 mM Tris-HCl, pH 7.4) and left to hydrate for 30 min

with gentle agitation. The liposomes were extruded with an Avanti Mini-Extruder (Avanti Polar Lipids, Alabaster, USA) and stored at 4°C in the dark.

Fluorescent liposomes (30% Dansyl-DOPE, 30% NBD-DOPC and 40% DOPG) were prepared from 1 mg of Dansyl-DOPE, 0.75 mg NBD-DOPC and 1 mg DOPG, respectively (Avanti Polar Lipids #810330c, #810132c and #840475c, respectively). Hydration and extrusion were performed at room temperature to a final concentration of 2.75 mg/mL and a diameter of 200 nm. DPPC and SM liposomes were prepared with the pure lipids (Avanti Polar Lipids DPPC #850355c, Egg-SM #860061c, respectively). Hydration was carried out at 50°C and 60°C, respectively, to a final concentration of 3 mg/mL. The liposomes were not extruded.

Cargo binding assay

Previously emptied P116 was incubated with an excess of donor liposomes; 2.8 µL of a 10 mM compound solution in DMSO; and 2.8 µL of a 510 µM peptide solution in buffer. The incubation was carried out in 50 µL total volume for 2 h at 37°C with mild shaking. Unbound cargo was removed by ultracentrifugation for 30 min at 150,000 x g in a Ti70 rotor with 1.5 mL Eppendorf tube adapters and re-ultracentrifugation of the upper 80% of supernatant, before collecting the upper 90% of supernatant and washing it three times in 50,000 MWCO centrifugal concentrators (Vivaspin 500, PES; Sartorius, Göttingen, Germany). Efficient removal was verified by MALDI-TOF mass spectrometry. Unspecific binding of compounds to the filter or tube wall was tested by repeating the procedure detailed above in the absence of protein. Binding of compounds to P116 via unspecific protein effects was tested by repeating the procedure detailed above in the presence of P110 and P140, *M. pneumoniae* membrane proteins.

Lipid transfer assay

To fill P116 with fluorescent lipids, 0.5 mg of emptied P116 was incubated with 50 µL of freshly extruded fluorescent donor liposomes (30% Dansyl-DOPE, 30% NBD-DOPC, 40% DOPG) for 2 h at 37°C with gentle shaking.

The fluorescent liposomes were then removed by ultracentrifugation for 30 min at 150,000 x g in a Ti70 rotor with 1.5 mL Eppendorf tube adapters and re-ultracentrifugation of the upper 80% of supernatant, before collecting the upper 90% of supernatant. Efficient removal was verified by MALDI-TOF mass spectrometry. The supernatant was concentrated using 10,000 MWCO centrifugal concentrators (Vivaspin 500, PES; Sartorius, Göttingen, Germany) to a volume <100 µL. It is important that the liposome-protein solution is re-suspended well by pipetting up and down before ultracentrifugation.

DPPC acceptor liposomes were prepared by 5x ultrafiltration in a 0.2 µm centrifugal concentrator (Vivaspin 500, PES; Sartorius) at 6,000 x g and dilution with liposome buffer. This eliminates smaller liposomes that would be lost in subsequent steps and cannot be imaged by the laser scanning microscope with a 63x/1.4 oil objective. Thorough re-suspension between rounds is crucial.

P116 filled with fluorescent lipids was incubated with DPPC acceptor liposomes for 2–16 h at room temperature with gentle shaking. P116 was then removed by washing four times with liposome buffer via ultrafiltration in 300,000 MWCO centrifugal concentrator (Vivaspin 500, PES) at 6,000 x g. The process was monitored by measuring the P116 concentration in the flow-through until total protein is recovered and the concentration in the filtrate is zero. A dot blot was used to verify that the concentration of P116 in the filtrate was << 0.5 µg. The resulting sample was subjected to analysis by MALDI-TOF mass spectrometry and laser-scanning microscopy. To account for spontaneous insertion of fluorescent lipids into the acceptor liposomes or

spontaneous fusion between acceptor and donor liposomes from possible donor liposome contaminations of the final sample, the procedure detailed above was repeated in the absence of P116, and the sample was subjected to analysis by laser-scanning microscopy. All experiments were carried out in triplicate, and all results could be replicated.

HaCaT cells were grown in DMEM with 10% FCS, thinly seeded in 8-well plates (ibidi, Gräfelfing, Germany) and allowed to adhere overnight. P116 filled with fluorescent lipids was added to the cells in serum-free DMEM and incubated overnight, for 2 h and for 30 min at 37°C. The cells were then washed three times with DMEM and left to recover for 2 h at 37°C in DMEM with 10% FCS.

Laser scanning microscopy

Laser-scanning fluorescence microscopy was performed on an inverse confocal microscope (LSM780, Axio Observer Z.1; Carl Zeiss, Jena, Germany) with a Plan-Aptochromat 63x/1.4 oil objective and Immersol 518F (Carl Zeiss, Jena, Germany) using laser lines at 405 nm and 458 nm. The pinhole was set to 1 airy unit. Imaging was done in an 8 µL drop of sample in an 8-well µ-Slide with glass bottom (ibidi). The fluorescence intensity of individual liposomes was analyzed with Zeiss ZEN 2012 (black) v.8.0.5.273 and ImageJ 1.53t[22].

Matrix-assisted laser desorption/ionization mass spectrometry

All samples were mixed in a 1:1 ratio with sDHB (Super-DHB; Bruker, Billerica, USA) matrix solution (50 mg mL in 50% acetonitrile (ACN), 50% water, and 0.1% trifluoroacetic acid). Subsequently, 1 µL aliquots of the mixture were deposited on a BigAnchor MALDI target (Bruker, Billerica, USA) and allowed to dry and crystallize at ambient conditions. MS spectra were acquired on a rapifleX MALDI-TOF/TOF (Bruker,

Billerica, USA) in the mass range of 100–2,000 m/z in reflector positive and negative mode for lipid measurements. The Compass 2.0 (Bruker, Billerica, USA) software suite was used for spectra acquisition and processing.

Single-particle cryo-EM

A 3.5 µL drop of purified P116 (300 µg/mL in 20 mM Tris, pH 7.4 buffer for peptide-filled P116 (30–957) and 3 mg/mL in 20 mM Tris, 0.5 mM CHAPSO, pH 7.4 buffer for P116 without the N-terminal domain (246–818)) was applied to a 45 s glow-discharged R1.2/1.3 C-flat grid (Electron Microscopy Science, Hatfield, USA), and plunge-frozen in liquid ethane (Vitrobot Mark IV; Thermo Fischer Scientific) at 100% relative humidity, 4°C, a nominal blot force of –3, a wait time of 0.5 s, and a blotting time of 12 s. Before freezing, Whatman 595 filter papers were incubated for 1 h in the Vitrobot chamber at 100% relative humidity and 4°C.

Dose-fractionated movies of peptide-filled P116 (30–957) and P116 (246–818) were collected with SerialEM v4.1.0beta[23] at a nominal magnification of 165,000 (0.819Å per pixel) in nanoprobe EFTEM mode at 300 kV with a Titan Krios (Thermo Fischer Scientific) electron microscope equipped with a GIF Quantum S.E. post-column energy filter in zero-loss peak mode and a K2 Summit detector (Gatan, Pleasanton, USA). For peptide-filled full-length P116 and P116 (246–818), a total of 6,077 and 4,314 micrographs with 22 and 50 frames per micrograph and a frame time of 0.2 and 0.1 s were collected, respectively. The camera was operated in dose-fractionation counting mode with a dose rate of ~8 electrons per $Å^2$ s^{-1}, resulting in a total dose of 60 electrons per $Å^2$. Defocus values ranged from –1 to –3.5 µm.

For emptied and refilled P116 (246–818), dose-fractionated movies were collected using EPU v.3.1.3 (Thermo Fischer Scientific) at a nominal magnification of 105,000 (0.837 Å/pix) in nanoprobe EFTEM mode at 300 kV with a Titan Krios G3i

electron microscope (Thermo Scientific) equipped with a BioQuantum-K3 imaging filter (Gatan) and operated in zero-loss peak mode with 30 eV energy slit width. In total, 8,002 micrographs with 50 frames per micrograph and a frame time of 0.05 s were collected. The K3 camera was operated in counting mode with a dose rate of ~15 electrons per $Å^2s^{-1}$, resulting in a total dose of 50 electrons per $Å^2$. Defocus values ranged from –0.8 to –3.5.

CryoSPARC v3.2[24] was used to process the cryo-EM data, unless stated otherwise. Beam-induced motion correction and contrast transfer function (CTF) estimation were performed using CryoSPARC's own implementation. For the dimers, particles were initially clicked with the Blob picker using a particle diameter of 200–300Å. Particles were then subjected to unsupervised 2D classification. For the final processing, the generated 2D averages were taken as templates for the automated particle picking. In total, 3,463,490 particles and 1,197,649 particles were picked and extracted with a binned box size of 256 pixels for peptide-filled P116 (30–957) and P116 (246–818), respectively. False-positive picks were removed by two rounds of unsupervised 2D classification. The dimerization rate of the core construct (246–818) was substantially less than that of the whole ectodomain (30–957), as evidenced by the presence of approximately 50% monomers in the 2D classes of the purified protein and >90% monomers in the 2D classes of the protein after emptying and refilling, compared with only dimers in the 2D class averages of the full-length ectodomain. The remaining 1,491,940 (peptide-filled P116 (30–957)) and 225,218 particles (P116 (246–818)) were used to generate an *ab initio* reconstruction with three classes followed by a heterogeneous refinement with three classes. For the final processing, 1,065,351 particles (peptide-filled P116 (30–957)) and 101,747 particles (P116 (246–818)) were used. For the remaining particles, the beam-induced specimen movement was corrected locally. The CTF was refined per group on the fly within the non-uniform

refinement[25]. The obtained global resolution of the homodimer was 3.3 Å for peptide-filled P116 (30–957) and 4.16 Å for P116 (246–818) (Extended Data Figure 1). For the monomers of P116 without the N-terminal domain (246–818), particles were initially clicked with the Blob picker using a particle diameter of 100–200 Å. Particles were then subjected to unsupervised 2D classification. For the final processing, the generated 2D averages were taken as templates for the automated particle picking. In total, 6,997,649 particles were picked and extracted with a box size of 256 pixels. False-positive picks were removed by two rounds of unsupervised 2D classification. The remaining 1,470,056 particles were used to generate an *ab initio* reconstruction with three classes followed by a heterogeneous refinement with three classes. For the final processing, 518,561 particles were used. For the remaining particles, the beam-induced specimen movement was corrected locally. The CTF was refined per group on the fly within the non-uniform refinement[25]. As initial volumes for the non-uniform refinement, maps were built with residues 246–818 from PDB: 8A9A (filled P116) and PDB:8A9B (empty P116) and filtered to 30 Å. Both maps yielded similar refined structures. The obtained global resolution of the monomer was 5.43 Å (Extended Data Figure 1).

Cryo-electron tomography of *M. pneumoniae*

Adherently growing *M. pneumoniae* cells overexpressing P116 were harvested by scraping 2 days after transformation without washing, and pelleting for 20 min at 15,000 x g. The pellet was washed once in 1 mL PBS, re-pelleted and then resuspended in 100 µL PBS. Multiple dilutions of the suspension were prepared and passed multiple times though a 25-gauge syringe needle until all clumps were resolved. The solution was mixed with fiducial markers (Protein A conjugated to 5 nm colloidal gold; Cell Biology Department, University Medical Center Utrecht, The

Netherlands) in some cases. From the solutions with or without fiducials, a 3.5 µL drop was applied to a (45 s) glow-discharged R1.2/1.3 C-flat grid (Electron Microscopy Science, Hatfield, USA) with a 4 nm carbon coat, and plunge-frozen in liquid ethane (Vitrobot Mark IV; Thermo Fischer Scientific) at 100% relative humidity, 4°C, and a nominal blot force of –1, with wait and blotting times of 8–12 s.

Tilt-series were recorded using SerialEM v4.0.14[23] at a nominal magnification of 81,000 (1.112 Å per pixel) in nanoprobe EFTEM mode at 300 kV with a Titan Krios G2 (Thermo Fischer Scientific) electron microscope equipped with a BioQuantum-K3 imaging filter (Gatan), operated in zero-loss peak mode with 20 eV energy slit width, and a K3 Summit detector (Gatan). The total dose per tomogram was 120 $e^{-}/Å^{2}$, and the tilt series covered an angular range from −60° to 60° with an angular increment of 3° and a defocus set at −3 µm. Local motion correction and CTF estimation of tilt series were done in Warp v.1.0.9[26]. Image stack alignment was done in IMOD v.4.11.8[27]. Tomograms were reconstructed in Warp v.1.0.9. Particles were clicked on deconvoluted tomograms in ArtiaX v1.0 (ChimeraX extension)[28]. Sub-tomograms were reconstructed with Warp, using the star files from ArtiaX after adding micrograph names and modifying the header. Initial models from sub-tomograms and 3D refinement were done with Relion v.3.1[29] with 698 homogenous and 1101 heterogeneous particles, a box size of 128 pixels, a pixel size of 4.445 Å/pix, a mask diameter of 450 Å, and a resolution of ~30 Å (EMD-18629). Filtered and projected sub-tomograms of individual particles were inspected in Amira v.5.3.3 (Thermo Fischer Scientific).

Molecular dynamics simulations

Atomistic simulation of the P116 dimer filled with cholesterol. We created an atomistic model of the P116 dimer (UniProt serial numbering, residues 60–868 per monomer) with each hydrophobic pocket filled with 12 cholesterols using UCSF Chimera[30]. We solvated the system with TIP3P water using GROMACS[31]. We minimized the system using the steepest-descent algorithm for 5000 steps and performed a 200-ps-long NVT equilibration using the V-rescale thermostat[32] with a reference temperature of 310 K (τt = 0.1 ps). We simulated the system in the NPT ensemble for 0.6 µs using the Charmm36m forcefield[33–35], a reference temperature of 310 K (τt = 1 ps, V-rescale thermostat), a reference pressure of 1 bar (τp = 5 ps, Parrinello-Rahman barostat[36]) and a NaCl concentration of 0.15 M. For both the van der Waals (Verlet) and the Coulomb forces (Particle Mesh Ewald), we used a $r_{cut-off} = 1.2\ nm$. We chose a 2 fs time step. We used GROMACS 2021.4.

Coarse-grained P116 dimer on membrane. First, we generated the MARTINI coarse-grained P116 dimer on a symmetrical bilayer membrane (30% DOPC, 30% DOPE, 40% DOPG) using the Charmm-GUI MARTINI maker webserver (bilayer builder) with the MARTINI 3.0 forcefield[37–39] on the PDB structure 8A9A (UniProt serial numbering, residues 60–868 per chain). We modified the elastic network generated by the software (via martinize2) to retain only intradomain bonds (we used this criterion for all the simulations). Using GROMACS 2021.4, we ran a 5000-step soft core (*free-energy* = *yes*) minimization followed by a 3000-step hard core (*free-energy* = *no*) minimization, both using the steepest descent algorithm. Then, we ran six rounds of NPT equilibration at a reference temperature of 310 K (V-rescale thermostat, τt = 1 ps) and a reference pressure of 1 bar (Berendsen barostat, semi-isotropic coupling type,

τp = 5 ps[40]) with ever-decreasing force constant on the position restraints of the membrane. We then simulated the system to obtain a docked conformation in NPT ensemble using GROMACS 2021.4 with 0.15 M NaCl at a reference temperature of 310 K (V-rescale thermostat, τt = 1 ps) and a reference pressure of 1 bar (Parrinello-Rahman barostat, semi-isotropic coupling type, τp = 5 ps). We used a time step of 20 fs.

We then took a docked conformation obtained with the previous run and used it to reinitialize the system where three lipids in proximity of the DCA of the docked P116 monomer were pulled towards the DCA using UCSF Chimera[30]. This was a first attempt to favor the lipid uptake. The new input model was solvated using the *insane.py* script[41]. We used a NaCl concentration of 0.15 M with neutralizing ions. We ran a 5000-step minimization using the steepest descent algorithm. Then, we ran an NPT equilibration at a reference temperature of 310 K (V-rescale thermostat, τt = 1 ps) and a reference pressure of 1 bar (Berendsen barostat, semi-isotropic coupling type, τp = 5 ps). We simulated this system in NPT ensemble using GROMACS 2021.4 at a reference temperature of 310 K (V-rescale thermostat, τt = 1 ps) and a reference pressure of 1 bar (Parrinello-Rahman barostat, semi-isotropic coupling type, τp = 5 ps) for about 35 μs. Coulombic interactions were treated with PME and a cut-off of 1.1 nm as for van der Waals interactions. We used a time step of 20 fs. During this simulation, P116 steadily docked to the membrane via residues F214 and F227 (see Figure 2d).

Coarse-grained P116 dimer on membrane with one flipped lipid tail. Based on a frame from the simulation of the P116 dimer steadily N-docked on the membrane, we created a model where one lipid tail was flipped to be in between the DCA helices and the other tail was inserted in the membrane bilayer. One lipid was deleted from the previous model to allow the positioning of the half-flipped lipid. This was achieved using

UCSF Chimera[30]. The new input model was solvated using the *insane.py* script[41]. We used a NaCl concentration of 0.15 M with neutralizing ions. We ran a 5000-step minimization using the steepest descent algorithm. Then, we ran an NPT equilibration at a reference temperature of 310 K (V-rescale thermostat, τt = 1 ps) and a reference pressure of 1 bar (Berendsen barostat, semi-isotropic coupling type, τp = 5 ps). We simulated this system in NPT ensemble using GROMACS 2021.4 at a reference temperature of 310 K (V-rescale thermostat, τt = 1 ps) and a reference pressure of 1 bar (Parrinello-Rahman barostat, semi-isotropic coupling type, τp = 5 ps). Coulombic interactions were treated with PME and a cut-off of 1.1 nm, as for van der Waals interactions. We used a time step of 20 fs.

Coarse-grained P116 dimer in solution with DOPG, DOPE and DOPC lipids. Using the topology of the P116 dimer and lipids from the simulations with membrane and the equilibrated P116 dimer configuration, we created the model of the P116 dimer with sealed hydrophobic pockets surrounded by 15 DOPGs, 7 DOPCs and 7 DOPEs using UCSF Chimera[30]. We then used the *insane.py* script[41] to solvate the system. We used a NaCl concentration of 0.15 M with neutralizing ions. Using GROMACS 2021.4, we ran a 5000-step minimization using the steepest descent algorithm. Then, we ran an NPT equilibration at a reference temperature of 310 K (V-rescale thermostat, τt = 1 ps) and a reference pressure of 1 bar (Berendsen barostat, semi-isotropic coupling type, τp = 5 ps). We simulated the system in the NPT ensemble using GROMACS 2021.4 with 0.15 M NaCl concentration at a reference temperature of 310 K (V-rescale, τt = 1 ps) and a reference pressure of 1 bar (Parrinello-Rahman barostat, isotropic coupling type, τp = 12 ps). Coulombic interactions were treated with PME and a cut-off of 1.1 nm, as for van der Waals interactions. We used a time step of 20 fs.

Definition of arc diameter, wringing angle, angle between N-terminal and core domains and reference structures. We defined the *arc diameter* of P116 as the average of the distances between residues 416 of chain A and 253 of chain B and between residues 253 of chain A and 416 of chain B per frame.

We defined the *wringing angle* ϕ as the angle between the planes containing the centers of mass of residues 280 and 301 and of the whole core domain of each monomer. We defined as offset the angle ϕ achieved when the two monomers were both facing approximately downwards (in general, in the same direction). We then subtracted this value from the raw values to set the *down-down conformation* at $\sim 0°$. Accordingly, we find that the *up-down conformation* is at $\sim 100°$.

We defined the *angle between the N-terminal domain and core domain* as the angle between the segments connecting the centers of mass of

- the residue pairs 164 and 181, and 107 and 108 and
- the residue pair 382 and 404 and the group 708 to 712.

We defined as *reference structures* the MARTINI CG model of the single-particle cryo-EM structure (PDB: 8A9A) and the CG model of the same structure after the finger helices had collapsed within the empty pocket during the production run. For this purpose, we did not modify the elastic network of the model, to keep the conformation as close as possible to the single-particle cryo-EM structure except for the open pocket.

References

20. Blötz, C. *et al.* Development of a replicating plasmid based on the native oriC in Mycoplasma pneumoniae. *Microbiology (Reading, England)* **164,** 1372–1382; 10.1099/mic.0.000711 (2018).

21. Hedreyda, C. T., Lee, K. K. & Krause, D. C. Transformation of Mycoplasma pneumoniae with Tn4001 by electroporation. *Plasmid* **30,** 170–175; 10.1006/plas.1993.1047 (1993).

22. Schindelin, J. *et al.* Fiji: an open-source platform for biological-image analysis. *Nature Methods* **9,** 676–682; 10.1038/nmeth.2019 (2012).

23. Mastronarde, D. N. Automated electron microscope tomography using robust prediction of specimen movements. *Journal of Structural Biology* **152,** 36–51; 10.1016/j.jsb.2005.07.007 (2005).

24. Punjani, A., Rubinstein, J. L., Fleet, D. J. & Brubaker, M. A. cryoSPARC: algorithms for rapid unsupervised cryo-EM structure determination. *Nature Methods* **14,** 290–296; 10.1038/nmeth.4169 (2017).

25. Punjani, A., Zhang, H. & Fleet, D. J. Non-uniform refinement: adaptive regularization improves single-particle cryo-EM reconstruction. *Nature Methods* **17,** 1214–1221; 10.1038/s41592-020-00990-8 (2020).

26. Tegunov, D. & Cramer, P. Real-time cryo-electron microscopy data preprocessing with Warp. *Nature Methods* **16,** 1146–1152; 10.1038/s41592-019-0580-y (2019).

27. Kremer, J. R., Mastronarde, D. N. & McIntosh, J. R. Computer visualization of three-dimensional image data using IMOD. *Journal of Structural Biology* **116,** 71–76; 10.1006/jsbi.1996.0013 (1996).

28. Ermel, U. H., Arghittu, S. M. & Frangakis, A. S. ArtiaX: An electron tomography toolbox for the interactive handling of sub-tomograms in UCSF ChimeraX. *Protein Science : a Publication of the Protein Society* **31,** e4472; 10.1002/pro.4472 (2022).

29. Scheres, S. H. W. RELION: implementation of a Bayesian approach to cryo-EM structure determination. *Journal of Structural Biology* **180,** 519–530; 10.1016/j.jsb.2012.09.006 (2012).

30. Pettersen, E. F. *et al.* UCSF Chimera—a visualization system for exploratory research and analysis. *Journal of Computational Chemistry* **25,** 1605–1612; 10.1002/jcc.20084. (2004).

31. van der Spoel, D. *et al.* GROMACS: fast, flexible, and free. *Journal of Computational Chemistry* **26,** 1701–1718; 10.1002/jcc.20291 (2005).

32. Bussi, G., Donadio, D. & Parrinello, M. Canonical sampling through velocity rescaling. *The Journal of Chemical Physics* **126,** 14101; 10.1063/1.2408420 (2007).

33. Guvench, O., Hatcher, E. R., Venable, R. M., Pastor, R. W. & Mackerell, A. D. CHARMM Additive All-Atom Force Field for Glycosidic Linkages between Hexopyranoses. *Journal of Chemical Theory and Computation* **5,** 2353–2370; 10.1021/ct900242e (2009).

34. Best, R. B. *et al.* Optimization of the additive CHARMM all-atom protein force field targeting improved sampling of the backbone φ, ψ and side-chain χ(1) and χ(2) dihedral angles. *Journal of Chemical Theory and Computation* **8,** 3257–3273; 10.1021/ct300400x (2012).

35. Guvench, O. *et al.* Additive empirical force field for hexopyranose monosaccharides. *Journal of Computational Chemistry* **29,** 2543–2564; 10.1002/jcc.21004 (2008).

36. Parrinello, M. & Rahman, A. Polymorphic transitions in single crystals: A new molecular dynamics method. *Journal of Applied Physics* **52,** 7182–7190; 10.1063/1.328693 (1981).

37. Periole, X., Cavalli, M., Marrink, S.-J. & Ceruso, M. A. Combining an Elastic Network With a Coarse-Grained Molecular Force Field: Structure, Dynamics, and Intermolecular

Recognition. *Journal of Chemical Theory and Computation* **5,** 2531–2543; 10.1021/ct9002114 (2009).

38. Hsu, P.-C. *et al.* CHARMM-GUI Martini Maker for modeling and simulation of complex bacterial membranes with lipopolysaccharides. *Journal of Computational Chemistry* **38,** 2354–2363; 10.1002/jcc.24895 (2017).

39. Qi, Y. *et al.* CHARMM-GUI Martini Maker for Coarse-Grained Simulations with the Martini Force Field. *Journal of Chemical Theory and Computation* **11,** 4486–4494; 10.1021/acs.jctc.5b00513 (2015).

40. Berendsen, H. J. C., Postma, J. P. M., van Gunsteren, W. F., DiNola, A. & Haak, J. R. Molecular dynamics with coupling to an external bath. *The Journal of Chemical Physics* **81,** 3684–3690; 10.1063/1.448118 (1984).

41. Wassenaar, T. A., Ingólfsson, H. I., Böckmann, R. A., Tieleman, D. P. & Marrink, S. J. Computational Lipidomics with insane: A Versatile Tool for Generating Custom Membranes for Molecular Simulations. *Journal of Chemical Theory and Computation* **11,** 2144–2155; 10.1021/acs.jctc.5b00209 (2015).